The ATP-waiting conformation of rotating F_1-ATPase revealed by single-pair fluorescence resonance energy transfer

Ryohei Yasuda*†, Tomoko Masaike‡§, Kengo Adachi¶, Hiroyuki Noji‖, Hiroyasu Itoh, and Kazuhiko Kinosita, Jr.¶**

*Cold Spring Harbor Laboratory, Cold Spring Harbor, NY 11724; ‡ATP System Project, Exploratory Research for Advanced Technology, Japan Science and Technology Corporation, 5800-3 Nagatsuta, Yokohama 226-0026, Japan; §Chemical Resources Laboratory, Tokyo Institute of Technology, 4259 Nagatsuta, Yokohama 226-8503, Japan; ¶Center for Integrative Bioscience, Okazaki National Research Institutes, Higashiyama 5-1, Myodaiji, Okazaki 444-8585, Japan; ‖Precursory Research for Embryonic Science and Technology, Japan Science and Technology Corporation, Institute of Industrial Science, University of Tokyo, 4-6-1 Komaba, Tokyo 153-8505, Japan; and **Hamamatsu Photonics KK, Tokodai, Tsukuba 300-2635, Japan

Edited by Paul D. Boyer, University of California, Los Angeles, CA, and approved June 16, 2003 (received for review December 23, 2002)

F_1-ATPase is an ATP-driven rotary motor in which a rod-shaped γ subunit rotates inside a cylinder made of $\alpha_3\beta_3$ subunits. To elucidate the conformations of rotating F_1, we measured fluorescence resonance energy transfer (FRET) between a donor on one of the three βs and an acceptor on γ in single F_1 molecules. The yield of FRET changed stepwise at low ATP concentrations, reflecting the stepwise rotation of γ. In the ATP-waiting state, the FRET yields indicated a γ position $\approx$40° counterclockwise (= direction of rotation) from that in the crystal structures of mitochondrial F_1, suggesting that the crystal structures mimic a metastable state before product release.

The F_1-ATPase is a part of F_oF_1-ATP synthase that synthesizes ATP in F_1, the water-soluble portion of the ATP synthase, from ADP and inorganic phosphate (P_i) when protons pass through F_o, the membrane-embedded portion. Isolated F_1, consisting of $\alpha_3\beta_3\gamma\delta\varepsilon$ subunits, hydrolyzes ATP as the reverse reaction. The minimum ATPase unit, $\alpha_3\beta_3\gamma$ (hereafter referred to as F_1), is pseudo 3-fold symmetric: a rod-shaped, asymmetric γ subunit is surrounded by an $\alpha_3\beta_3$ cylinder (1). Rotation of γ inside the $\alpha_3\beta_3$ cylinder has been suggested (2–5) and confirmed by chemical (6) and optical (7, 8) methods. Direct observation under an optical microscope (8–11) has shown that F_1 rotates in discrete 120° steps, each fueled by a single ATP molecule.

Several kinds of high-resolution crystal structures of mitochondrial F_1 (MF_1) have been solved (1, 12, 13), but it is unknown which rotation states these crystal structures correspond to or how closely these are related to the structure of actively rotating F_1. To investigate the transient structures in rotating F_1, we applied a single-pair fluorescence resonance energy transfer (FRET) technique (14). We measured FRET between a donor (Cy3) on one of three βs and an acceptor (Cy5) on γ in single thermophilic F_1 molecules fixed on a glass surface (Fig. 1). Because the FRET yield strongly depends on the distance between the two fluorophores, the FRET yield will change cyclically as the γ subunit rotates (15). The distance between labeled residues were estimated from the FRET yield and used to analyze the transient conformation of F_1.

Materials and Methods

Proteins. Cy5-maleimide was prepared as in ref. 16. The sole cysteine of a mutant subcomplex of F_1, α(C193S)$_3\beta$(His-10 tag at N terminus)$_3\gamma$(S107C) derived from thermophilic *Bacillus* PS3, was labeled with Cy5-maleimide (molar ratio 1:2) in 20 mM Mops-KOH (pH 7.0), 100 mM KCl, and 5 mM glycine at 23°C for 30 min. The cysteine of a mutant β(S205C) (without His tag) was labeled with Cy3-maleimide at 1:2 in the same buffer excluding glycine at 23°C for 30 min. Free dyes were removed on a PD10 column (Amersham Pharmacia). The (Cy5-γ)F_1 was incubated with Cy3-β at 1:10 at 45°C for 2 days, and free β subunit was removed on a size exclusion column (Superdex 200, Amersham Pharmacia). The final preparation contained 0.7–1 mol Cy5 and 0.05–0.2 mol Cy3 per mol F_1 (estimated from absorption spectra, using ε_{555}^{Cy3} = 150,000 $M^{-1}\cdot cm^{-1}$, ε_{555}^{Cy5} = 15,000 $M^{-1}\cdot cm^{-1}$, ε_{655}^{Cy5} = 250,000 $M^{-1}\cdot cm^{-1}$, ε_{280}^{Cy3} = 15,000 $M^{-1}\cdot cm^{-1}$, ε_{280}^{Cy5} = 25,000 $M^{-1}\cdot cm^{-1}$, and $\varepsilon_{280}^{F_1}$ = 154,000 $M^{-1}\cdot cm^{-1}$). A solution of 0.05–0.5 nM labeled F_1 in 50 mM KCl, 2 mM $MgCl_2$, 10 mM Mops-KOH (pH 7.0), 0.06–1 μM ATP, 70 mM 2-mercaptoethanol, 200 μg/ml glucose oxidase, 20 μg/ml catalase, and 4.5 mg/ml glucose was sandwiched between two KOH-cleaned quartz coverslips for microscopic observation. Resulting thickness of the solution was $\approx$3 μm. Previously, we found that His-tagged F_1 rotates on a clean glass surface (11), presumably bound by the negatively charged surface. To determine the activity of labeled β, a construct α(C193S)$_3\beta$(S205C)$_3\gamma$(S107C) was expressed and labeled with Cy3 at 1:8–20, resulting in 0.5–1.0 mol of Cy3 per cysteine. ATPase activity was measured as described (9).

Microscope. A laser beam (532 nm, DPSS 532–200, Coherent Radiation, Palo Alto, CA) was introduced into an inverted microscope (IX70, Olympus) through a water-immersion objective (PlanApo ×60, numerical aperture 1.2, Olympus). Fluorescence was divided into <620-nm (Cy3) and >620-nm (Cy5) components (17) and focused onto an intensified (VS4–1845, Videoscope, Dallas) charge-coupled device (CCD-300T-IFG, Dage-MTI, Michigan City, IN) camera. Bandpass filters (Chroma Technology, Brattleboro, VT) reduced the cross talk between Cy3 and Cy5 channels to <3%. The excitation efficiency of Cy5 at 532 nm was <0.03 times that of Cy3. Images recorded on a videotape were captured in a personal computer (LG3, Scion, Frederick, MD) and analyzed off-line with custom software. Because only Cy5 close to a donor emitted fluorescence, we could find FRET pairs (F_1 having both Cy3 and Cy5) by looking for fluorescence of Cy5. Most FRET pairs (>99%) did not show time-dependent change of the FRET yield, presumably because of surface denaturation (18). In the Cy3 channel, we observed many more fluorescent spots that lack companion spots in the Cy5 channel. Most of them photobleached in a single step. These presumably represent F_1 carrying a single Cy3 fluorophore without Cy5 acceptor.

Calculation of Distance Between FRET Pairs. The FRET yield f was obtained experimentally as $f = a\text{Cy5}/(\text{Cy3} + a\text{Cy5})$, where Cy5 and Cy3 denote the fluorescence intensities above the background and a is the ratio of the intensity change of two dyes,

This paper was submitted directly (Track II) to the PNAS office.

Abbreviations: FRET, fluorescence resonance energy transfer; MF_1, mitochondrial F_1; DCCD, dicyclohexylcarbodiimide.

†To whom correspondence should be addressed. E-mail: yasuda@cshl.org.

www.pnas.org/cgi/doi/10.1073/pnas.1637860100

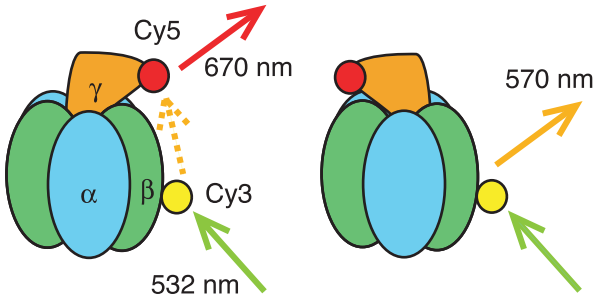

Fig. 1. Visualization of the rotation of F_1 through single-pair FRET: principle of the experiment.

ΔCy3/ΔCy5 (see Fig. 3*E*). The distance between the donor and acceptor was calculated as $R = R_o(1/f - 1)^{1/6}$, where f is the experimental FRET yield and R_o is the Förster distance (19). R_o was determined as $[(8.79 \times 10^{17}) \cdot n^{-4} \cdot \kappa^2 \cdot Q_D \cdot J]^{1/6}$ (nm), where J, the overlap integral, was calculated from measured emission spectrum of (Cy5-γ)F_1 and absorption spectrum of (Cy3-β)F_1 to be 8.85×10^{-13} $M^{-1} \cdot cm^3$, $Q_D = 0.25$ is the quantum yield of the donor measured with rhodamine-B (quantum yield = 0.49; ref. 20) as reference, $n = 1.33$ is the refractive index of water, and $\kappa^2 = 0.667 \pm 0.524$ (see below) is the orientation factor. The error in R_o was mainly from κ^2 and was estimated as $\delta R_o = R_o \cdot \delta(\kappa^2)/(6\kappa^2)$. Resulting R_o was 5.9 ± 0.8 nm. The error in R was estimated as $(R_o^6/6R^5f^2)\delta f + (R/R_o)\delta R_o$, where δf is the standard error for f.

Calculation of Orientation Factor. The orientation factor κ^2 is defined as $\kappa^2 = \langle(cos\theta_T - 3\, cos\theta_D\, cos\theta_A)^2\rangle$, where θ_T is the angle between $\boldsymbol{\mu}_D$ and $\boldsymbol{\mu}_A$, the donor emission and acceptor absorption transition moments, and θ_D is the angle between $\boldsymbol{\mu}_D$ and $\boldsymbol{d}$ and θ_A between $\boldsymbol{\mu}_A$ and $\boldsymbol{d}$, where $\boldsymbol{d}$ is the vector connecting the donor and acceptor (19). Because none of these angles are known, we assigned arbitrary orientations to $\boldsymbol{\mu}_D$, $\boldsymbol{\mu}_A$, and $\boldsymbol{d}$ and calculated average κ^2 for that combination while allowing $\boldsymbol{\mu}_D$ and $\boldsymbol{\mu}_A$ to wobble within a cone around the assigned axis. This calculation was repeated for all combinations of $\boldsymbol{\mu}_D$, $\boldsymbol{\mu}_A$, and $\boldsymbol{d}$, giving the average and standard deviation for κ^2. The cone angle ϕ_X (X = A or D) for the subnanosecond wobble of the fluorophore is related to the limiting and residual fluorescence anisotropy r_o and r_{inf} (21) by $r_{inf} = r_o \cdot [cos\phi_X(1 + cos\phi_X)/2]^2$. r_o and r_{inf} in turn are related with the steady-state anisotropy r_s (21) by $r_s = (r_o - r_{inf})/(1 + \tau/\tau_r) + r_{inf}$, in which τ is the fluorescence lifetime and τ_r the rotation correlation time of the dye. τ/τ_r was estimated, by assuming that τ_r is not much different from the correlation time of free dye in water, as $(\tau/\tau_r)_{water} Q_{protein}/Q_{water}$, where $Q_{protein}$ and Q_{water} are the quantum yields of the dye on protein and in water, and $(\tau/\tau_r)_{water}$ is the quantity for free dye in water that was measured as $(\tau/\tau_r)_{water} = (r_o/r_{water} - 1)$, where r_{water} is the steady-state anisotropy of the free dye in water. The steady-state fluorescence anisotropy r_s was measured in a cuvette by using a spectrofluorometer (F-4500, Hitachi, Tokyo) to be 0.29, 0.30, 0.26, and 0.17 for (Cy3-β)F_1 (some proteins contain multiple Cy3), (Cy5-γ)F_1, free Cy3, and free Cy5, respectively (λ_{ex} = 550 and 650 nm, λ_{em} = 590 and 690 nm, respectively for Cy3 and Cy5). Lower limit of r_o (giving lower limit of the cone angle) was measured as the steady-state anisotropy of the dyes in glycerol at 0°C to be 0.36 for Cy3 and 0.39 for Cy5. The quantum yield Q was measured as 0.25, 0.26, 0.03, and 0.25, respectively, for Cy3-F_1, Cy5-F_1, free Cy3, and free Cy5, using rhodamine-B as a reference. From measured r_s, r_o, and Q, the wobble cone semiangles were obtained as $\phi_D > 25°$ and $\phi_A > 33°$ for Cy3 and Cy5 on F_1.

Derivation of Possible Positions of FRET Pair. The linker length from the dye center to the labeled cysteine sulfur was estimated to be 1.2 and 1.7 nm for Cy3 and Cy5, respectively, from the bond angles and lengths. The donor and acceptor were assumed to be within the linker lengths of the labeled cysteines (β205 and γ107; β203 and γ99 in the MF_1 sequence). Because γ97–100 in MF_1 are unresolved in the crystals, possible positions of γ99-S (mutated to cysteine) were calculated as follows: the peptide backbone was extended from the visible γ101 to γ99 by assigning standard bond lengths and angles while allowing arbitrary rotations around N—C_α (Φ) and C—C_α (Ψ) bonds. If resultant γ99-C is not within 1.0 nm (maximum possible length between γ99-C and γ96-C) from γ96-C, the structure was discarded. Carbonyl oxygens and amino nitrotgens and γ99-C_β were modeled automatically assuming the standard L-amino acid configuration (no need to model a side chain for γ100 glycine). Finally, C_α—C_β bond in γ99 was rotated into an arbitrary angle to locale γ99S. During the construction, if an added atom (excluding hydrogen) was within 0.15 nm of the visible atoms in the crystal, that structure was also discarded. After 5,000 trials, we obtained 562, 462, and 2,323 possible γ99S locations for native MF_1, (ADP AlF_4^-)$_2MF_1$, and MF_1-dicyclohexylcarbodiimide (DCCD). For each location, we assigned a sphere of radius 1.7 nm and assumed that the acceptor could be anywhere in the sphere with the same probability. The acceptor spheres seen in Fig. 5 show the outermost circumference enclosing all possible acceptor position. In the native MF_1 (1), γ91–96 and γ101 are also missing, and we adopted the (ADP AlF_4^-)$_2MF_1$ structure (12) for this part.

Positions of the acceptor compatible with our FRET results (see Fig. 5 *A* and *B*, red dots) were obtained as follows. First, we randomly assigned a donor position from the donor sphere, removing the positions inside the protein by discarding the positions within 0.4 nm of the atoms in the crystal structure. We also chose $\boldsymbol{\mu}_D$ and $\boldsymbol{\mu}_A$ randomly. Instead of rotating the acceptor, we rotated the donor into three equivalent positions, assuming the same linker vector and $\boldsymbol{\mu}_D$ for the three (simple 120° rotations). Then we selected three FRET efficiency values f, one for a high-FRET state and two for low-FRET states, assuming a Gaussian distribution for f with half-width at $1/e$ maximum equaling the experimental standard error. The remaining task was to find three donor-acceptor vectors $\boldsymbol{d}$ that are compatible with the chosen conditions. This was done in an iterative search for the orientation and absolute value of $\boldsymbol{d}$ by first assigning random orientations to the three vectors $\boldsymbol{d}$. (*i*) We calculated three orientation factors from the chosen orientations of $\boldsymbol{d}$, $\boldsymbol{\mu}_D$, and $\boldsymbol{\mu}_A$, while allowing $\boldsymbol{\mu}_D$ and $\boldsymbol{\mu}_A$ to wobble in the respective cones. (*ii*) This gave three distances $|\boldsymbol{d}|$, from which we determined the acceptor position. Two answers were obtained, above and below F_1, and we always chose the one above. (*iii*) From the acceptor position, we extracted three orientations of $\boldsymbol{d}$, disregarding the absolute values, and repeated steps *i*-*iii*. We stopped the iteration when the differences in the three orientations between two adjacent iteration cycles all became $<0.5°$. In $\approx$10% of trials, the calculation did not converge within 500 iterations and we gave up. For a chosen set from $\approx$1,800 donor positions, $\boldsymbol{\mu}_D$ and $\boldsymbol{\mu}_A$, we always attempted five independent iterations starting from different and randomly selected orientations of $\boldsymbol{d}$. These gave consistent results within 0.2 ± 0.04 nm (mean $\pm$ SD), when converged. Finally, if the obtained acceptor position was within 0.4 nm of the crystal atoms that position was discarded (to avoid physical conflicts). Red dots seen in Fig. 5 *A* and *B* represent results obtained in this way. When we rotated γ for a better fit with the experimental FRET efficiencies (see Fig. 5), the final check of physical conflicts was made for each γ orientation; the number of remaining red dots did not depend significantly on the γ angle, ranging from 1,340 to 1,414, 1,144 to 1,308, and 1,078 to 1,187, respectively, for native MF_1, (ADP AlF_4^-)$_2MF_1$, and MF_1-DCCD.

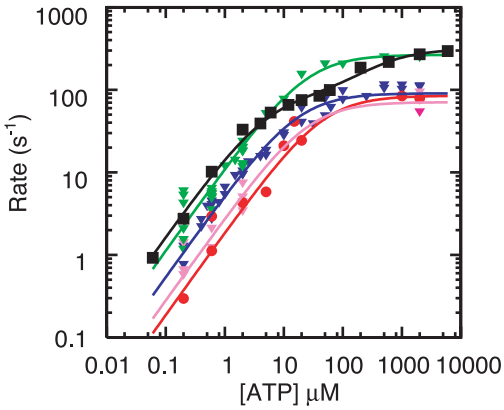

Fig. 2. Effect of labeling on ATPase activity (11). F_1 with a sole cysteine at γ was labeled with Cy3 (green) or unlabeled (black). F_1 with four cysteines (one each in βs and γ) were fully labeled (red), 50% labeled (pink), or unlabeled (blue). Smooth curves are fits with $V_{max}[ATP]/([ATP] + k_M)$ (green, red, pink, blue) or with $(V_{max}k_M + V_{max2}[ATP]^2)/([ATP]^2 + k_{M2}[ATP] + k_Mk_{M2})$ (black). The rate of ATP binding, k_{on}, was estimated as $V_{max}/k_M = (1.1 \pm 0.3) \times 10^7\ M^{-1}{\cdot}s^{-1}$ (green), $(5.4 \pm 0.9) \times 10^6\ M^{-1}{\cdot}s^{-1}$ (blue), $(1.9 \pm 1.1) \times 10^6\ M^{-1}{\cdot}s^{-1}$ (red), $(2.8 \pm 1.2) \times 10^6\ M^{-1}{\cdot}s^{-1}$ (pink), and $(1.65 \pm 0.32) \times 10^7\ M^{-1}{\cdot}s^{-1}$ (black).

The probability of finding a FRET-compatible acceptor position (see red dots in Fig. 5 *A* and *B*) among the possible acceptor positions in the crystal structures was estimated by counting the number of red dots within the acceptor-linker length of a possible γ99-S position, averaging this number over all possible γ99-S positions, and dividing the average by the total number of the red dots. We also calculated the probabilities for rotated γ by rotating the acceptor spheres.

Results

Visualization of F_1 Rotation Through Single-Pair FRET. To label one of the three βs with Cy3 (Fig. 1), we expressed β alone with an engineered cysteine and labeled it with Cy3. The labeled β was exchanged into an independently expressed F_1 of which γ had been labeled with Cy5, resulting in 0.05–0.2 mol of labeled β and 0.7–1.0 mol of labeled γ per mol of F_1. The effect of β mutation and labeling was checked in yet another F_1 construct where all three βs had the cysteine and were fully labeled (Fig. 2): at low [ATP] where hydrolysis rate was proportional to [ATP], the apparent rate of ATP binding was estimated as $k_{on}^{labeled} = 1.9 \times 10^6\ M^{-1}{\cdot}s^{-1}$ and $k_{on}^{unlabeled} = 1.7 \times 10^7\ M^{-1}{\cdot}s^{-1}$ for the labeled and unlabeled F_1. When only one of three β was labeled, therefore, the rotation at low [ATP] where ATP binding is rate limiting will consist of alternate one slow and two fast steps, as has been demonstrated for an F_1 chimera of normal and slow β subunits (22).

Under an epi-fluorescence microscope, Cy3 was selectively excited at 532 nm, and emissions from Cy3 and Cy5 were simultaneously imaged. The two showed alternate and stepwise intensity changes in the presence of ATP (Fig. 3 *A–C*), indicating alternation of the FRET yield between high and low states. The rate of alternation was faster at higher [ATP], as expected for ATP-dependent stepwise rotation of γ. When Cy3 lost its companion acceptor by photobleaching of Cy5, the fluorescence of Cy3 increased (arrow in Fig. 3*A*). If Cy3 bleaches before Cy5, both are expected to disappear simultaneously, as was indeed observed (arrows in Fig. 3 *B* and *C*). There was a clear correlation between Cy3 and Cy5 fluorescence, showing the existence of two FRET states (Fig. 3 *D–F*).

The transition rates between the high- and low-FRET states, defined as the inverse of the averaged dwell times, ($1/\langle\tau_H\rangle$ and $1/\langle\tau_L\rangle$), were each proportional to [ATP] (Fig. 4), confirming that the change in the FRET yield represents rotation steps. The

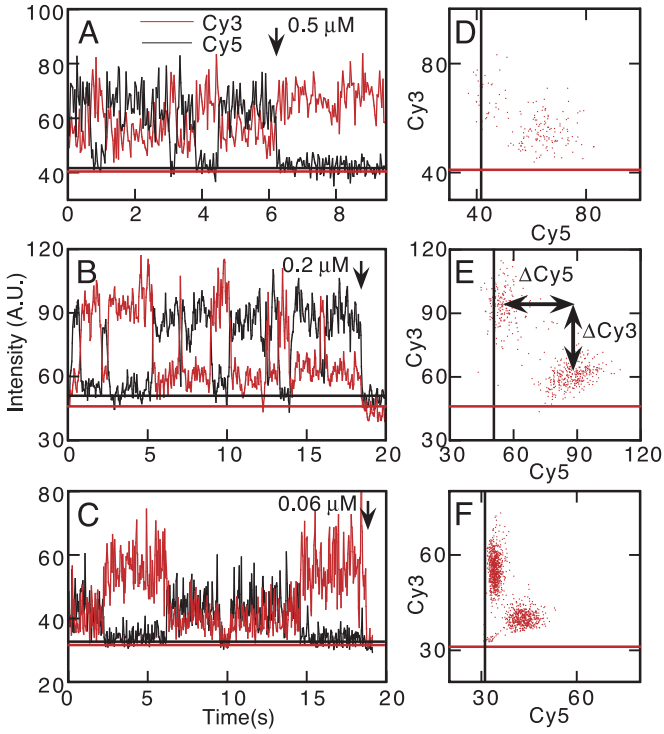

Fig. 3. Changes in the FRET yield accompanying rotation. (*A–C*) Time courses of Cy3 (red) and Cy5 (black) fluorescence at different [ATP]. Arrows indicate photobleaching of Cy5 (*A*) or Cy3 (*B* and *C*). (*D–F*) Correlation between Cy3 and Cy5 intensities in *A–C* (data up to the arrow are scored). Straight lines in *A–F* represent the background intensities for Cy3 (red) and Cy5 (black) channels measured near the FRET pair.

rate of rotation, estimated as $1/(\langle\tau_H\rangle + \langle\tau_L\rangle)$, was also proportional to [ATP] (Fig. 4*A*).

For 120° stepping, three FRET states are expected, as observed for a different donor-acceptor pair (15). In our experiments, two of three states were indistinguishable, leading to two possibilities: (*i*) the high-FRET state with a longer dwell ($\langle\tau_H\rangle/\langle\tau_L\rangle = 2.3 \pm 0.3$) involved one slow step associated with the labeled β and the low-FRET state involved two normal steps, or (*ii*) the high-FRET state involved one normal and one slow steps and the low-FRET state involved one normal step. For each case, the rates of ATP binding, $k_{on}^{labeled}$ and $k_{on}^{unlabeled}$ were calculated from the observed dwell times and compared with the rates estimated from ATP hydrolysis. For case *i*, $k_{on}^{labeled}$ is given as $\langle\tau_H\rangle^{-1}[ATP]^{-1} = (3.8 \pm 0.7) \times 10^6\ M^{-1}{\cdot}s^{-1}$ and $k_{on}^{unlabeled}$ as $2\langle\tau_L\rangle^{-1}[ATP]^{-1} = (1.6 \pm 0.3) \times 10^7\ M^{-1}{\cdot}s^{-1}$, both of which agree with $k_{on}^{labeled}$ and $k_{on}^{unlabeled}$ estimated from the ATPase activity. For case *ii*, $k_{on}^{labeled} = (\langle\tau_L\rangle - \langle\tau_H\rangle)^{-1}[ATP]^{-1} = (7.4 \pm 3.8) \times 10^6\ M^{-1}{\cdot}s^{-1}$ and $k_{on}^{unlabeled} = \langle\tau_L\rangle^{-1}[ATP]^{-1} = (7.8 \pm 1.3) \times 10^6\ M^{-1}{\cdot}s^{-1}$, inconsistent with the ATPase results. Thus, the low-FRET state involved two normal steps, and the high-FRET state involved one slow step. Histograms of dwell times (Fig. 4*B*) were also better fit with model *i*.

ATP-Waiting Conformation of F_1. The FRET yields in the high- and low-FRET states were calculated from the observed fluorescence intensities as 0.56 ± 0.06 and 0.15 ± 0.03, respectively, corresponding to the donor-acceptor distances of 5.7 ± 0.9 and 7.9 ± 1.0 nm. Because the low-FRET state involves two rotation steps, the distance between the two dyes will change as 5.7, 7.9, and 7.9 nm during rotation. These values are to be compared with the known crystal structures of F_1.

Three different crystal structures of MF_1 have been solved: a

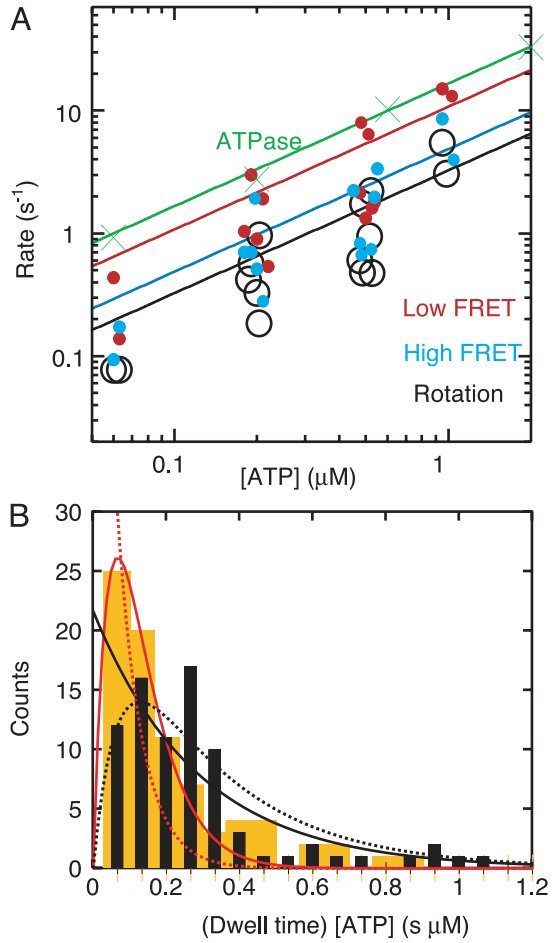

Fig. 4. (*A*) ATP dependence of the transition rate from the high and low FRET states ($1/\langle\tau_H\rangle$ and $1/\langle\tau_L\rangle$) and the rotation rate estimated as $1/(\langle\tau_H\rangle + \langle\tau_L\rangle)$ (160 FRET states were analyzed in 15 FRET pairs). For comparison, the rate of ATP hydrolysis in F_1 without the subunit labeling is shown (Fig. 2*A*). Lines show linear fits with slopes (± SE) of (4.9 ± 0.7), (10.9 ± 1.3), (3.3 ± 0.4), and (16.5 ± 0.2) × 10^6 $M^{-1}\cdot s^{-1}$ for $1/\langle\tau_H\rangle$, $1/\langle\tau_L\rangle$, rotation, and ATPase, respectively. (*B*) Histogram of dwells, τ, of the high (black) and low (orange) FRET states. Solid curves show fit for case *i* in the text: low FRET dwell (red) with $constant\cdot\tau[ATP]\exp(-k_{on}^{unlabeled}\tau[ATP])$, where $k_{on}^{unlabeled} = 1.65 \times 10^7\ M^{-1}\cdot s^{-1}$ is the ATP binding constant of unlabeled F_1 from Fig. 2, and high FRET dwells (black) with $constant\cdot\exp(-k_{on}^{labeled}\tau[ATP])$, where $k_{on}^{labeled} = 1.9 \times 10^6\ M^{-1}\cdot s^{-1}$ is for labeled β ($\chi^2 = 257$, 80 dwells, 15 FRET pairs). Dashed curves show fit for case *ii* in the text: low FRET dwells (red) with $constant\cdot\exp(-k_{on}^{unlabeled}\tau[ATP])$, and high FRET dwells (black) with $constant\cdot\{\exp(-k_{on}^{labeled}\tau[ATP]) - \exp(-k_{on}^{unlabeled}\tau[ATP])\}$, where $k_{on}^{labeled}$ and $k_{on}^{unlabeled}$ are fixed to the experimental values above ($\chi^2 = 497$, 80 dwells, 15 FRET pairs).

"native MF_1" structure in which AMP-PNP, ADP, and none occupy the three catalytic sites (1), an "MF_1-DCCD" structure that is inhibited with DCCD and has the same nucleotides as the native MF_1 (12), and an "$(ADP\ AlF_4^-)_2MF_1$" structure, which is inhibited with aluminum fluoride and has two ADP AlF_4^- and one ADP (13). To compare these structures, we adopt the triangle made of three α-carbons of α-GLU26 as the frame of reference (23); a line perpendicular to, and passing through the center of, the triangle is assumed to be the rotation axis. The conformation of γ inside the $\alpha_3\beta_3$ cylinder varies little among the three crystal structures, whereas part of γ near the upper orifice of the $\alpha_3\beta_3$ cylinder is twisted clockwise (opposite to the rotation direction) up to 20° and 11° in $(ADP\ AlF_4^-)_2MF_1$ and MF_1-DCCD, respectively, compared with the native MF_1 when viewed from above in Figs. 1 and 5 (13).

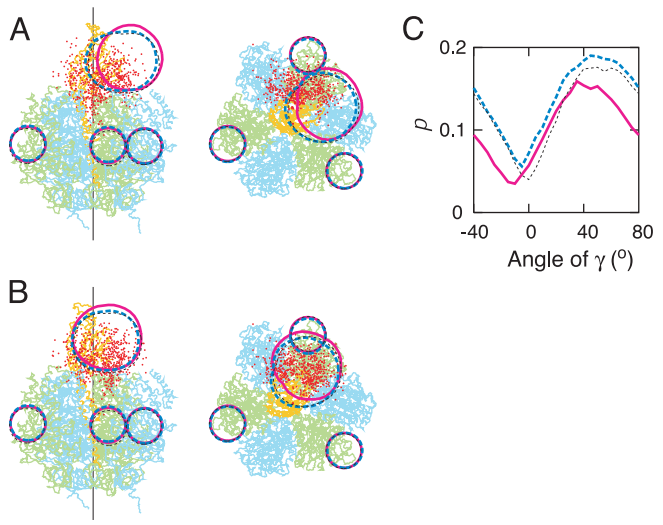

Fig. 5. (*A*) Side (*Left*) and top (*Right*) views of the backbone trace of the structure of $(ADP.AlF_4^-)_2$ MF_1 (13), color-coded as in Fig. 1*A*. Small and large spheres represent geometrically allowed positions of the donor (Cy3) and acceptor (Cy5), respectively, on the native MF_1, $(ADP\ AlF_4^-)_2MF_1$, and MF_1-DCCD structures (blue, black, and pink); the degree of twist in γ varies among the three structures, resulting in the slight deviations of large circles. Red dots indicate possible acceptor positions calculated from the FRET results (see *Materials and Methods*). The black line indicates the putative rotation axis. (*B*) The acceptor sphere (and γ) is rotated counterclockwise by 40°. (*C*) Probability (p) of finding red dots in the acceptor sphere as functions of γ angle (θ) for native MF_1 (blue), MF_1-DCCD (pink), and $(ADP\ AlF_4^-)_2$ MF_1 (black). Larger values between $p(\theta)$ and $p(\theta + 120°)$ are plotted.

In these structures, the position of the residue labeled with the acceptor, which is on the protruding portion of γ, varies to some extent, while the donor residues occupy the same positions. Possible positions of the donor and acceptor in the three MF_1 structures are essentially the same (Fig. 5*A*, small and large spheres for the donor and acceptor, respectively). The acceptor spheres are larger, because several residues around the acceptor site are unresolved in the structures and linker length of the acceptor is longer than that of the donor. Starting with the donor positions that are common to all structures, we calculated acceptor positions that are compatible with the three FRET efficiencies above (red dots in Fig. 5 *A* and *B*). The FRET-estimated acceptor positions overlap best with the acceptor sphere (large ones) when γ was rotated counterclockwise by ≈40° in all MF_1 crystals (Fig. 5*C*). Because FRET measurements were done at low ATP concentrations where binding of ATP limits the rotation rate, this conformation corresponds to the ATP-waiting state of F_1.

Discussion

Rotation Mechanism of F_1-ATPase. Our FRET results suggest that the conformation of γ in the ATP-waiting state of F_1 is ≈40° counterclockwise, or ≈40° in the rotation direction, from that in the MF_1 crystal structures. Then, which kinetic state do the MF_1 structures correspond to? At least one intermediate state during rotation, other than the ATP-waiting state, has so far been resolved: binding of ATP to F_1 in the ATP-waiting state induces a counterclockwise ≈90° substep, and F_1 remains at this intermediate angle for ≈2 ms before undergoing a further ≈30° substep induced by product release (11). When F_1 is inhibited on tight binding of MgADP, the rotation stalls at ≈80° (24), suggesting that the inhibited conformation resembles that of the intermediate state after the ≈90° substep. Naively, crystal structures are expected to be close to the 90°/80° conformation rather than the ATP-waiting conformation, because crystalliza-

tion involves long incubation with MgADP or MgATP, a condition that favors the formation of the MgADP-inhibited enzyme (25), as has been suggested in cross-linking studies (26). If so, expected acceptor positions in the ATP-waiting state should be 30°/40° ahead the crystal structures (Fig. 5*B*). Our FRET results (Fig. 5, red dots) indeed point to this position, suggesting that the crystal structures are closer to the 90°/80° conformation rather than the ATP-waiting conformation (0° or 120°).

Whether rotation of F_1-ATPase requires filling of all three catalytic sites with a nucleotide (27) or filling two is sufficient (28) is an important, but unresolved, issue. Because γ orientation in both the 2- and 3-nt crystal structures differ from our results by 40°, the ATP-waiting conformation likely binds a single nucleotide. If so, rotation under our experimental conditions occurs by filling at most two catalytic sites.

The protruding part of γ in crystals of F_1 from *Escherichia coli* (29) or the thermophilic bacterium (Y. Shirakihara, personal communication) is twisted counterclockwise compared with the MF_1 structures, such that possible acceptor positions in these bacterial crystals are close to the large circles in Fig. 5*B*. Our FRET results obtained with the thermophilic F_1 are consistent with these positions. In particular, the thermophilic bacterial crystal contained only 1 nt, suggesting again that the ATP-waiting state corresponds to a single-nucleotide state.

Our interpretations above rest on the assumption that the crystal structures closely mimic an active rotation intermediate hosting the same number of nucleotides. However, the lattice packing may have deformed the F_1 structure in the crystals (12, 13). The twist of γ in (ADP AlF_4^-)$_2MF_1$ and MF_1-DCCD, relative to native MF_1, is maximal around the orifice of the $\alpha_3\beta_3$ cylinder and is smaller both above and below the orifice, suggesting some distortion. In particular, native MF_1 and MF_1-DCCD both have two catalytic nucleotides, and yet γ in MF_1-DCCD is twisted clockwise up to 11°. Significantly, the MF_1-DCCD crystal is more closely packed than the native MF_1 crystal, and the bacterial crystals in which γ is twisted counterclockwise are less densely packed. A possibility thus exists that 2-nt MF_1 in a relaxed crystal might show a γ orientation similar to the bacterial one. If so, our FRET results might point to the necessity of three-site filling. FRET with different donor-acceptor pairs will help resolve the remaining ambiguity.

Analysis of Protein Conformation Through Single-Pair FRET. FRET is a standard technique for measuring distances in the 1- to 10-nm range and often used for analyzing conformation of proteins and nucleotides in solution (30). For analysis of transient protein conformations, FRET measurement on individual donor-acceptor pairs is essential because protein molecules behave stochastically and their operations cannot be synchronized.

In this study, we have demonstrated that single-pair FRET reveals a transient conformation of F_1-ATPase with nanometer precision. The resolution, limited mainly by the ambiguity in the orientation factor and the relatively large linker length between the fluorophore and target residue, could be improved by synthesizing short-linker fluorophores and searching for a proper fluorophore-residue combination that warrants an extensive wobble of the fluorophore on the protein surface.

We thank T. Nishizaka, T. Ariga, and Y. Shirakihara for critical discussions. This work was supported by the Japan Society for the Promotion of Science (to R.Y.), the Burroughs Wellcome Fund (to R.Y.), Core Research for Evolutional Science and Technology, and Grants-in-Aid from the Ministry of Education, Science, Sports, and Culture of Japan.

1. Abrahams, J. P., Leslie, A. G., Lutter, R. & Walker, J. E. (1994) *Nature* **370,** 621–628.
2. Boyer, P. & Kohlbrenner, W. (1981) in *Energy Coupling in Photosynthesis*, eds. Selman, B. R. & Selman-Reimer, S. (Elsevier, Amsterdam), pp. 231–240.
3. Cox, G., Jans, D. A., Fimmel, A., Gibson, F. & Hatch, L. (1984) *Biochim. Biophys. Acta* **849,** 62–69.
4. Oosawa, F. & Hayashi, S. (1986) *Adv. Biophys.* **22,** 151–183.
5. Boyer, P. D. (2000) *Biochim. Biophys. Acta* **1458,** 252–262.
6. Duncan, T. M., Bulygin, V. V., Zhou, Y., Hutcheon, M. L. & Cross, R. L. (1995) *Proc. Natl. Acad. Sci. USA* **92,** 10964–10968.
7. Sabbert, D., Engelbrecht, S. & Junge, W. (1996) *Nature* **381,** 623–625.
8. Noji, H., Yasuda, R., Yoshida, M. & Kinosita, K., Jr. (1997) *Nature* **386,** 299–302.
9. Yasuda, R., Noji, H., Kinosita, K., Jr., & Yoshida, M. (1998) *Cell* **93,** 1117–1124.
10. Adachi, K., Yasuda, R., Noji, H., Itoh, H., Harada, Y., Yoshida, M. & Kinosita, K., Jr. (2000) *Proc. Natl. Acad. Sci. USA* **97,** 7243–7247.
11. Yasuda, R., Noji, H., Yoshida, M., Kinosita, K., Jr., & Itoh, H. (2001) *Nature* **410,** 898–904.
12. Gibbons, C., Montgomery, M. G., Leslie, A. G. W. & Walker, J. E. (2000) *Nat. Struct. Biol.* **7,** 1055–1061.
13. Menz, R. I., Walker, J. E. & Leslie, A. G. (2001) *Cell* **106,** 331–341.
14. Kelley, A., Michalet, X. & Weiss, S. (2001) *Science* **292,** 1671–1672.
15. Börsch, M., Diez, M., Zimmermann, B., Reuter, R. & Graber, P. (2002) *FEBS Lett.* **527,** 147–152.
16. Funatsu, T., Harada, Y., Tokunaga, M., Saito, K. & Yanagida, T. (1995) *Nature* **374,** 555–559.
17. Kinosita, K., Jr., Itoh, H., Ishiwata, S., Hirano, K., Nishizaka, T. & Hayakawa, T. (1991) *J. Cell Biol.* **115,** 67–73.
18. Kinosita, K., Jr., Yasuda, R., Noji, H. & Adachi, K. (2000) *Philos. Trans. R. Soc. London B* **355,** 473–489.
19. Förster, T. (1948) *Annalen Physik* **2,** 55–75.
20. Ishikawa, M., Hirano, K., Hayakawa, T., Shigeru, H. & Brenner, S. (1994) *Jpn. J. Appl. Phys.* **33,** 1571–1576.
21. Kinosita, K., Jr., Kawato, S. & Ikegami, A. (1984) *Adv. Biophys.* **17,** 147–203.
22. Ariga, T., Masaike, T., Noji, H. & Yoshida, M. (2002) *J. Biol. Chem.* **277,** 24870–24873.
23. Wang, H. & Oster, G. (1998) *Nature* **396,** 279–282.
24. Hirono-Hara, Y., Noji, H., Nishiura, M., Muneyuki, E., Hara, K. Y., Yasuda, R., Kinosita, K., Jr., & Yoshida, M. (2001) *Proc. Natl. Acad. Sci. USA* **98,** 13649–13654.
25. Milgrom, Y. M. & Boyer, P. D. (1990) *Biochim. Biophys. Acta* **1020,** 43–48.
26. Tsunoda, S. P., Muneyuki, E., Amano, T., Yoshida, M. & Noji, H. (1999) *J. Biol. Chem.* **274,** 5701–5706.
27. Weber, J. & Senior, A. E. (2001) *J. Biol. Chem.* **276,** 35422–35428.
28. Boyer, P. D. (2002) *FEBS Lett.* **512,** 29–32.
29. Hausrath, A. C., Gruber, G., Matthews, B. W. & Capaldi, R. A. (1999) *Proc. Natl. Acad. Sci. USA* **96,** 13697–13702.
30. Selvin, P. R. (2000) *Nat. Struct. Biol.* **7,** 730–734.